Editors' Suggestion

Black Hole Quasibound States from a Draining Bathtub Vortex Flow

Sam Patrick,[1,*] Antonin Coutant,[1,†] Maurício Richartz,[2,‡] and Silke Weinfurtner[1,§]
[1]School of Mathematical Sciences, University of Nottingham, Nottingham NG7 2FD, United Kingdom
[2]Centro de Matemática, Computação e Cognição, Universidade Federal do ABC (UFABC), 09210-170 Santo André, São Paulo, Brazil

(Received 2 February 2018; revised manuscript received 16 May 2018; published 7 August 2018)

Quasinormal modes are a set of damped resonances that describe how an excited open system is driven back to equilibrium. In gravitational physics these modes characterize the ringdown of a perturbed black hole, e.g., following a binary black hole merger. A careful analysis of the ringdown spectrum reveals the properties of the black hole, such as its angular momentum and mass. In more complex gravitational systems, the spectrum might depend on more parameters and hence allows us to search for new physics. We present a hydrodynamic analog of a rotating black hole that illustrates how the presence of extra structure affects the quasinormal mode spectrum. The analogy is obtained by considering wave scattering on a draining bathtub vortex flow. We show that due to vorticity of the background flow, the resulting field theory corresponds to a scalar field on an effective curved spacetime which acquires a local mass in the vortex core. The obtained quasinormal mode spectrum exhibits long-lived trapped modes, commonly known as quasibound states. Our findings can be tested in future experiments building upon recent successful implementations of analog rotating black holes.

DOI: 10.1103/PhysRevLett.121.061101

Introduction—The linear response of a perturbed black hole can be well understood in terms of damped resonances called quasinormal modes (QNMs) [1,2]. These damped modes possess a complex frequency whose real part corresponds to the oscillation frequency and whose imaginary part gives the lifetime. The QNM spectrum of a black hole is completely characterized by the black hole parameters, and it does not depend on the initial conditions of the perturbations. With the ongoing development of gravitational wave astronomy, significant efforts are being dedicated to use QNM spectra to reveal information about the structure of black holes, thereby allowing us to test general relativity and alternative theories of gravity [3]. In this Letter, we shall illustrate how the QNM spectrum can be drastically altered by additional structures in the context of analog gravity.

Analog gravity, pioneered by Unruh in 1981 [4], explores the possibility of testing gravitational effects in a broad variety of systems [5]. For instance, it was shown in Ref. [6] that surface waves propagating on an inviscid, irrotational, and shallow fluid flow are equivalent to a scalar field propagating on an effective spacetime. This spacetime is completely determined by its propagation speed c and the background fluid flow $\mathbf{v}$. In particular, it is possible to model a rotating black hole using an axisymmetric fluid flow $\mathbf{v}(r) = v_r(r)\mathbf{e}_r + v_\theta(r)\mathbf{e}_\theta$. The fluid configuration will exhibit an ergosphere at $r = r_e$ if $|\mathbf{v}(r_e)| = c$ and an event horizon at $r = r_H$ if $|v_r(r_H)| = c$. These two features are sufficient to give rise to many interesting effects that occur around astrophysical black holes, including Hawking radiation and superradiance [5]. In particular, this allows us to experimentally test the universality and robustness of these effects. The past decade has seen an increase of interest in experimental realizations of analog black holes, resulting in the measurement of both classical [7–9] and quantum [10] analog Hawking radiation in $(1+1)$-dimensional systems. Experimental research on rotating, $(2+1)$-dimensional systems began more recently and is already bearing fruit. For example, superradiant amplification of surface waves was observed in a draining bathtub (DBT) vortex flow [11]. Rotating black hole analogs are also being explored using photon fluids [12].

In this Letter, we present a simplified model of a rotational DBT-type fluid flow motivated by realistic velocity profiles [11,13,14] seen in experiments. Our model is also the analog of a black hole with additional structure owing to the nonvanishing vorticity of the background flow in the center of the vortex. Within our approximation, the vorticity causes perturbations to acquire a local effective mass close to the horizon. This is similar to certain studies of gravity, where a massless field can acquire a local mass by coupling to another field [15,16]. By studying the QNM spectrum, we find that our model admits long-lived trapped modes in addition to the usual QNMs. These are known in the literature as quasibound states (QBSs) [1] and are predicted to occur in particular for massive fields around Kerr black holes [17,18]. Our findings are of relevance for both hydrodynamics and gravity. Our aim is to understand the consequences of additional structures on the QNM spectrum. The question arises in gravity when one

introduces modifications to the usual Kerr metric [19], as well as in fluid flows where the core structure of a vortex deviates from the irrotational case. With analog gravity experiments gaining an increasing amount of momentum, it is likely that the challenge of measuring the QNM spectrum will be tackled in the near future. In order to perform such experiments, it is necessary to understand the dependence of the QNM spectrum on the specifics of the background flow.

Background flow and wave equation.—The DBT vortex is a particularly simple hydrodynamic model based on the assumption of a highly symmetric flow. It is described by the irrotational and incompressible velocity profiles $v_\theta = C/r$ and $v_r = -D/r$, where C (circulation) and D (drain rate) are positive constants, and (r, θ) are the polar coordinates. The associated effective metric mimics a rotating black hole as it possesses a horizon at $r_H = D/c$, and an ergosphere at $r_e = \sqrt{C^2 + D^2}/c$. Its QNM spectrum has been studied in the literature, see, e.g., Refs. [20–23].

Even though the DBT model successfully describes the behavior of the flow sufficiently far from the center, a vortex which forms under experimental conditions contains a core in which the flow is no longer irrotational. A more realistic formula for v_θ is given by the Rankine vortex (originally conceived for gases, this model is now widely used for all types of viscous fluids [24])

$$v_\theta = \frac{Cr}{r_0^2}\Theta(r_0 - r) + \frac{C}{r}\Theta(r - r_0), \tag{1}$$

where r_0 is the radius of the vortex core and Θ is the Heaviside step function. An analytically amenable interpolation of this formula, which is a smooth function of r, was proposed by Rosenhead [25] and later studied by Mih and co-workers [26–28],

$$v_\theta = \frac{Cr}{r_0^2 + r^2}. \tag{2}$$

Notice that there exist many more complicated models, offering a more accurate description of the vortex flow depending on the precise initial and boundary conditions of the flow [24]. In this Letter, we are interested in the main deviations introduced by a rotational core. Hence, we will work with Eq. (2), as its analytic simplicity will lend itself to our frequency domain simulations. Since we are dealing with a two-dimensional axisymmetric model, the radial component is constrained by the incompressibility condition, which leads to the same radial velocity as in the DBT vortex, i.e., $v_r = -D/r$. Using these velocity profiles, we investigate the QNM spectrum.

The equations governing an effective $(2+1)$-dimensional ideal fluid flow in the shallow water regime (single layer approximation [29]) are given by

$$\begin{aligned}(\partial_t + \mathbf{v}\cdot\boldsymbol{\nabla})\mathbf{v} + g\nabla h = 0,\\ (\partial_t + \mathbf{v}\cdot\boldsymbol{\nabla})h + h\boldsymbol{\nabla}\cdot\mathbf{v} = 0.\end{aligned} \tag{3}$$

These equations are valid in the regime $h \ll L$, where h is the height of the free surface and L is the scale of variation in the (r, θ) plane. Perturbations $\mathbf{u}$ to the background velocity can be expressed using a Helmholtz decomposition, $\mathbf{u} = \boldsymbol{\nabla}\phi + \tilde{\boldsymbol{\nabla}}\psi$, where the cogradient operator is defined as $\tilde{\boldsymbol{\nabla}} = \mathbf{e}_z \times \boldsymbol{\nabla}$, and $\mathbf{e}_z$ is the unit vector in the direction perpendicular to the $(2+1)$-dimensional fluid ($\tilde{\boldsymbol{\nabla}}$ can also be seen as the curl of the three-dimensional vector field $\psi\mathbf{e}_z$). In the regime of short wavelengths $\lambda \ll L$ (but still shallow water $h \ll \lambda$), which amounts to a WKB approximation, the curl-free component obeys the wave equation

$$(\partial_t + \mathbf{v}\cdot\boldsymbol{\nabla})^2\phi + \Omega_v^2\phi - c^2\nabla^2\phi = 0, \tag{4}$$

and the other component is obtained through $(\partial_t + \mathbf{v}\cdot\boldsymbol{\nabla})\psi = -\Omega_v\phi$. Moreover, the surface elevation δh can be obtained from

$$g\delta h = -(\partial_t + \mathbf{v}\cdot\boldsymbol{\nabla})\phi + \Omega_v\psi. \tag{5}$$

In particular, the frequency content of δh and ϕ will be identical. Equation (4) describes the propagation of a scalar field ϕ with a mass proportional to the background vorticity $\Omega_v = \tilde{\boldsymbol{\nabla}}\cdot\mathbf{v}$. We note that wave equation (4) becomes exact in two particular cases. The first is a solid body rotation $\mathbf{v} \propto r\mathbf{e}_\theta$ with $\Omega_v = \text{const}$, in which case the perturbations are called inertia gravity waves [29]. The second is an irrotational flow, in which case $\Omega_v = 0$ and the wave equation reduces to its standard form [30]. The problem of waves scattering on a Rankine-type vortex has been addressed in the literature, usually in the regime $|\mathbf{v}| \ll c$ [31,32]. In our case, the effects we are interested in arise in the regime where $|\mathbf{v}|$ is on the order of c.

Since the velocity profile, we assume, is axisymmetric and stationary, Eq. (4) can be solved by separation of variables. Hence, a generic perturbation can be written as a sum $\phi = \sum_{\omega m}\phi_{\omega m}(r)\exp(im\theta - i\omega t)/\sqrt{r}$, where m is the azimuthal number and ω the frequency. To simplify, one can perform a Boyer-Lindquist–type transformation (see, e.g., Ref. [22]) and introduce a radial tortoise coordinate r_* through $dr_* = cdr/(c^2 - v_r^2)$. Using this coordinate, the horizon is located at $r_* \to -\infty$, while at large r, we have $r_* \sim r$. The wave equation for a single frequency and azimuthal number reduces to

$$-\partial_{r_*}^2\phi_{\omega m} + V(r)\phi_{\omega m} = 0, \tag{6}$$

where the effective potential V is given by

$$V(r) = -\left(\omega - \frac{m v_\theta}{r}\right)^2 + \left(c^2 - \frac{D^2}{r^2}\right) \times \left(\frac{m^2 - \frac{1}{4}}{r^2} + \frac{5D^2}{4c^2 r^4} + \frac{\Omega_v^2}{c^2}\right). \quad (7)$$

This differs from the usual potential since we are now using Eq. (2) for v_θ and the nonvanishing vorticity contributes the term Ω_v^2, where $\Omega_v = \partial_r(r v_\theta)/r$. Since the potential is symmetric under the transformation $\{\omega \to -\omega, m \to -m\}$, we restrict ourselves to $\mathrm{Re}(\omega) > 0$ in the frequency domain. Hence, co- (counter-) rotating waves are defined by $m > 0$ ($m < 0$).

The QNM boundary conditions are that the wave is purely ingoing on the horizon and purely outgoing at spatial infinity. By solving Eq. (6) in the corresponding limits $r_* \to -\infty$ and $r_* \to \infty$, the boundary conditions can be expressed as

$$\phi_{\omega m} \to \begin{cases} A_\infty e^{i\omega r_*}, & r_* \to \infty, \\ A_H e^{-i(\omega - m\Omega_H) r_*}, & r_* \to -\infty, \end{cases} \quad (8)$$

where A_∞ and A_H are constants, and Ω_H is the angular frequency $\Omega_H = (v_\theta/r)|_{r=r_H}$ at the horizon.

Computing quasinormal modes.—Solving the wave equation subject to the boundary conditions (8) selects a discrete set of complex frequencies $\omega = \omega^R + i\Gamma$. Several methods are known in the literature to accomplish this objective [1]. We study the problem using three distinct methods. We start with a WKB method which allows us to make the distinction between the QNMs and QBSs and to approximate their frequencies. Next, we implement a frequency domain simulation using a continued-fraction method which allows us to accurately compute the quasinormal frequencies to six-digit precision. Our last approach is a direct time domain simulation of Eq. (4) giving the time evolution of an initial perturbation of the vortex flow. Such a time evolution could be directly tested in future experiments. As we show, all three methods give consistent results. (In addition, by setting $r_0 = 0$, we have checked that all three methods reproduce the irrotational QNM spectrum for the DBT profile [22,33].)

WKB method.—In the WKB regime (which is valid particularly for $|m| \gg 1$) solutions are accurately described by a wave $\phi_{\omega m} \sim A \exp[i \int k(r_*) dr_*]$, where A is a slowly varying amplitude and $k(r_*)$ is the local wave number which obeys the Hamilton-Jacobi equation

$$k^2(r_*) = -V(r_*) \doteq [\omega - \omega_+(r_*)][\omega - \omega_-(r_*)], \quad (9)$$

with

$$\omega_\pm = \frac{m v_\theta}{r} \pm \sqrt{\left(c^2 - \frac{D^2}{r^2}\right)\left(\frac{m^2 - \frac{1}{4}}{r^2} + \frac{5D^2}{4c^2 r^4} + \frac{\Omega_v^2}{c^2}\right)}, \quad (10)$$

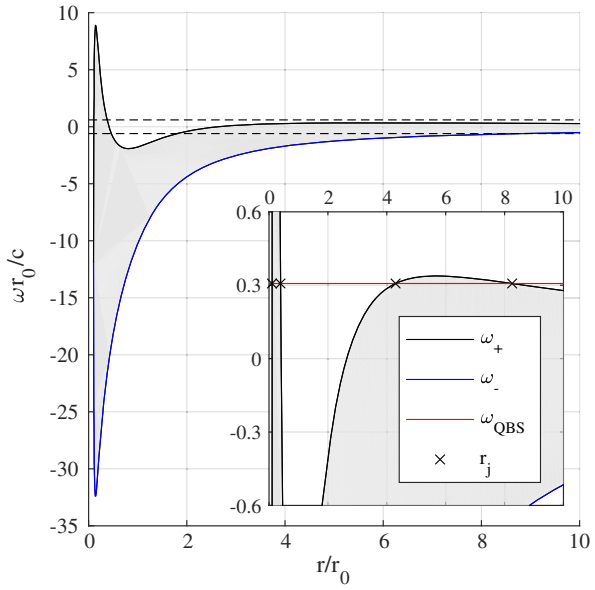

FIG. 1. We plot the functions $\omega_+(r)$ (black curve) and $\omega_-(r)$ (blue curve) defined in Eq. (10) for the dimensionless parameters $C/cr_0 = 3$, $D/cr_0 = 0.1$ and for the $m = -4$ mode. The region between the dashed lines is shown in the inset to highlight the presence of the smaller peak. The QNM frequencies are approximately those satisfying $\omega_\pm = \omega$, $\omega_\pm' = 0$. A QBS frequency is shown for illustrative purposes. The turning points of the QBS are the r_j values with $j = 1, \ldots, 4$ moving from left to right in the figure.

where r is understood to be a function of r_*. The two functions $\omega_\pm$ conveniently represent the potential (7) for varying values of ω (see Fig. 1). Indeed, at the level of the WKB approximation, we see that if ω lies outside the range $[\omega_-, \omega_+]$, then $k^2 > 0$. Hence, the solution is oscillatory and the wave propagates. On the contrary, if ω is inside this range, where $k^2 < 0$, the solution is evanescent. Moreover, points for which $\omega = \omega_\pm$ correspond to turning points. If, in addition, the point is a local extremum of $\omega_\pm$, it is an equilibrium point. Since we restrict ourselves to $\omega > 0$, it is sufficient to consider the extrema of ω_+.

Near a local maximum, waves can hover around the vortex analog of a light ring [22,34]. The real part of the QNM frequencies can be approximated through the conditions $\omega = \omega_+$ at the location such that $\omega_+' = 0$, where the prime denotes the derivative with respect to r_*. In the eikonal limit ($|m| \gg 1$), this condition is fulfilled at a single (m independent) radius r_{lr}, which is the light ring. Its orbital frequency $\omega_{\mathrm{lr}} = \omega_+|_{r_* = r_{\mathrm{lr}}}$ governs the QNM spectrum according to the formula [35]

$$\omega_{\mathrm{QNM}} = m\omega_{\mathrm{lr}} - i\left(n + \frac{1}{2}\right)\sqrt{\frac{-2V''}{(\partial_\omega V)^2}}, \quad (11)$$

where $n \in \mathbb{Z}$ is called the overtone number and the term under the square root is evaluated at $r = r_{\mathrm{lr}}$, $\omega = \omega_{\mathrm{lr}}$. In the

potential of Eq. (6), there are two maxima, and hence two associated families of QNMs.

In addition to the usual QNMs, the existence of two peaks in the scattering potential means that QBSs can also exist in the system. These QBSs can be understood as trapped modes in the potential well that must tunnel across the peaks to decay. Hence, the characteristic lifetimes of these modes are significantly larger than those of QNMs.

To estimate the frequency of these QBSs, we perform a scattering amplitude calculation using WKB modes everywhere except at the turning points. We then construct a global solution using connection formulas at the turning points. When a QBS exists, the scattering potential contains four turning points $(r_{*j})_{j=1,\ldots,4}$ (see Fig. 1). We define I_d, I_1, and I_2 as the ranges spanned by the dip and the two peaks, respectively; for example, $I_d = [r_{*2}, r_{*3}]$. The real part ω_n^R of the QBS frequencies are given by the Bohr-Sommerfeld condition

$$S_d(\omega_n^R) = \pi(n + 1/2), \tag{12}$$

where $S_d(\omega_n^R) = \int_{I_d} \sqrt{|V(\omega_n^R, r)|}dr_*$ is the WKB action evaluated over the range I_d and $n \in \mathbb{Z}$ indexes the different energy levels in the dip. In contrast to QNMs, this relation is satisfied only by a finite number of ω_n^R values.

Once the real part is determined, the imaginary part Γ_n of a long-lived mode with $\Gamma_n \ll \omega_n^R$ is given by

$$\Gamma_n = -\frac{T_1^2 \pm T_2^2}{4\partial_\omega S_d|_{\omega=\omega_n^R}}, \tag{13}$$

where the transmission coefficients across the inner (1) and outer (2) potential barriers are given by $T_{1,2} = \exp(-S_{1,2})$ in the WKB regime, and $S_{1,2}$ are the actions evaluated over the ranges $I_{1,2}$. In Eq. (13) we take the minus sign if $\omega^R < m\Omega_H$, corresponding to a superradiant amplification on the inner barrier, and the plus sign otherwise. By comparing Eqs. (11) and (13), we see that the lifetimes of QBSs are typically exponentially large compared to those of QNMs. A full derivation of Eqs. (12) and (13) is outlined in the Supplemental Material [36].

Numerical simulations.—Our first numerical method is a direct time domain simulation of Eq. (4) using a Gaussian pulse parallel to one of the Cartesian axes as initial data. The wave equation is numerically integrated using the method of lines (MOL) and a fourth-order Runge-Kutta algorithm. The quasinormal frequencies are extracted by performing a time Fourier transform of the signal once the initial pulse has passed. The second method is a frequency domain simulation implemented through a continued-fraction method (CFM) [37,38]. The two methods are detailed in the Supplemental Material [36].

Results.—In Fig. 2 we present our main results. We use the MOL simulations to reconstruct the full two-dimensional pattern $\phi(r, \theta)$ [Fig. 2(a)] and its decomposition in azimuthal modes $\phi_m(r)e^{im\theta}$ [Figs. 2(b1)–2(b5)] at fixed time after the initial pulse has passed the vortex. We also present the real [Fig. 2(c1)] and imaginary [Fig. 2(c2)] components of the complex frequency spectrum obtained by the three different methods. We observe excellent agreement between the results from the MOL (red crosses) and the CFM (blue diamonds) simulations. The WKB approximation then allows us to identify the underlying structure of the spectrum, i.e., whether the mode is a QNM (solid black dots) or a QBS (solid green dots). We show that most of the excited modes are QBSs and that, as a result, the ringdown has a significantly prolonged lifetime.

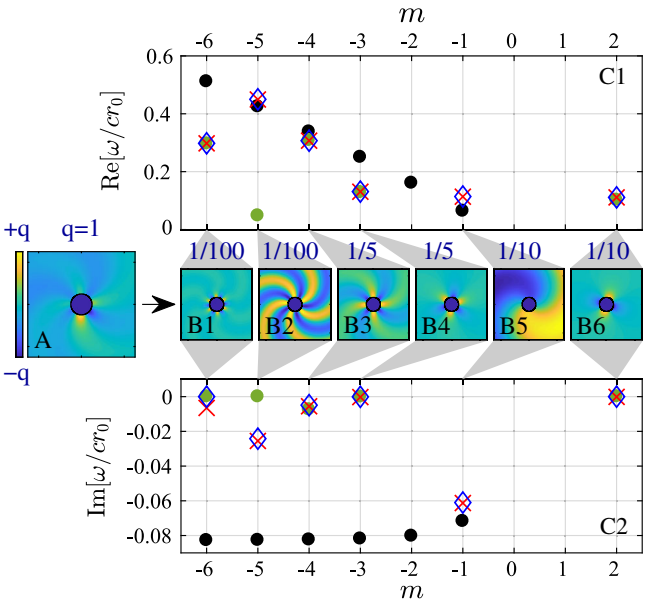

FIG. 2. Results obtained for the fluid flow parameters $C/cr_0 = 3$, $D/cr_0 = 0.1$. (a) The ringdown obtained from the MOL simulation of a initial Gaussian wave packet after it has passed the vortex. (b1)–(b6) The decomposition of the ringdown signal onto an azimuthal basis for $m \in \{-6, -5, -4, -3, -1, +2\}$. We display only the values of m for which the signal is above the noise level. To show the relative amplitudes of each component, we refer to a common color bar rescaled by a factor q [indicated above each of the panels (b1)–(b6)], normalized to 1 for the overall signal [panel (a)]. (c1),(c2) The real and imaginary parts of the complex frequency spectrum obtained by the three methods: MOL (red crosses), CFM (blue diamonds), and WKB (green dots for QBSs and black dots for the usual QNMs). The MOL and the CFM are in excellent agreement. Moreover, by comparing the MOL and the CFM with the WKB results, we see that only $m = -1$ is a usual QNM, while $m \in \{-6, -4, -3, +2\}$ indicates QBSs. Note that the distinction between the usual QNMs and QBSs close to the peaks in the scattering potential is not sharply defined, as in the case of the $m = -5$ mode here.

Conclusion.—Our results show that the core structure of a vortex can significantly affect its QNM spectrum, providing a fluid analog of the problem of spectral stability in black hole physics [19]. Specifically, a decrease in the angular velocity in the vortex core creates a local minimum

in the effective scattering potential which supports new resonances called quasibound states (the origin of these states is the same as for bound states of massive fields around Kerr black holes). Furthermore, we argue that the main effect of vorticity of the background on the propagation of waves can be encoded in a quantity which preserves the causal structure of the geometry, namely, an effective local mass [see Eq. (4)]. This is similar to scalar-tensor theories of gravity, where scalar perturbations also possess a spatially varying effective mass. In addition, the conclusions drawn in this paper should be observable experimentally by analyzing the ringdown of a vortex flow. If the core of the vortex lies behind the horizon ($r_0 < r_H$), then the observed spectrum will be close to that of an ideal DBT. On the contrary, if the core is large enough ($r_0 > r_H$), our results show that the presence of QBSs will significantly alter the time response of the system by allowing long-lived modes to hover around the vortex. As a last remark, we notice that QBSs, and even bound states, will also appear if the analog black hole is encompassed by a circular rigid boundary [45]. In our Letter, however, we demonstrate that vorticity alone is sufficient to trap modes around the analog black hole and produce QBSs.

We end this Letter by sketching a possible experimental setup to test our predictions. For this, we suggest a draining vortex flow similar to Ref. [11] but shallower [such that the 2D effective description leading to Eq. (3) becomes accurate]. To better control the rotation, a rotating plate can be added at the bottom of the tank with a drain hole in its center. The radius of the plate allows one to control r_0. Indeed, above it, viscous effects will impose a fluid velocity profile equal to that of the plate (that is, a solid body rotation as in the center of the Rankine vortex). By stimulating the vortex with a wave pulse, one will excite the QNMs and QBSs.

The ringdown we described above would manifest itself as rotating spirals imprinted on the free surface. In fact, such spirals are known to appear frequently around vortex flows (see Fig. 1 of the Supplemental Material [36]), for which a theoretical description seems to be lacking in the literature. We believe that the study of resonance frequencies could provide a fair description of this phenomenon.

The authors would like to thank Emanuele Berti, Thomas Sotiriou, and Théo Torres for the illuminating discussions. This project has received funding from the European Union's Horizon 2020 research and innovation program under Marie Skł odowska-Curie Grant Agreement No. 655524. M. R. acknowledges partial support from the São Paulo Research Foundation (FAPESP), Grant No. 2013/09357-9, and from the Fulbright Visiting Scholars Program. M. R. is also grateful to the University of Mississippi for its hospitality while part of this research was being conducted. S. W. acknowledges financial support provided under the Royal Society University Research Fellowship (Grant No. UF120112), the Nottingham Advanced Research Fellowship (Grant No. A2RHS2), the Royal Society Project (Grant No. RG130377), Royal Society Enhancement Grant No. RGF/EA/180286, and EPSRC Project Grant No. EP/P00637X/1. S. W. acknowledges partial support from STFC Consolidated Grant No. ST/P000703.

*sampatrick31@googlemail.com
†antonin.coutant@nottingham.ac.uk
‡mauricio.richartz@ufabc.edu.br
§silkiest@gmail.com

[1] E. Berti, V. Cardoso, and A. O. Starinets, Classical Quantum Gravity **26**, 163001 (2009).
[2] R. A. Konoplya and A. Zhidenko, Rev. Mod. Phys. **83**, 793 (2011).
[3] N. Yunes, K. Yagi, and F. Pretorius, Phys. Rev. D **94**, 084002 (2016).
[4] W. G. Unruh, Phys. Rev. Lett. **46**, 1351 (1981).
[5] C. Barceló, S. Liberati, and M. Visser, Living Rev. Relativity **14**, 3 (2011).
[6] R. Schützhold and W. G. Unruh, Phys. Rev. D **66**, 044019 (2002).
[7] S. Weinfurtner, E. W. Tedford, M. C. J. Penrice, W. G. Unruh, and G. A. Lawrence, Phys. Rev. Lett. **106**, 021302 (2011).
[8] F. Belgiorno, S. L. Cacciatori, M. Clerici, V. Gorini, G. Ortenzi, L. Rizzi, E. Rubino, V. G. Sala, and D. Faccio, Phys. Rev. Lett. **105**, 203901 (2010).
[9] L.-P. Euvé, F. Michel, R. Parentani, T. G. Philbin, and G. Rousseaux, Phys. Rev. Lett. **117**, 121301 (2016).
[10] J. Steinhauer, Nat. Phys. **12**, 959 (2016).
[11] T. Torres, S. Patrick, A. Coutant, M. Richartz, E. W. Tedford, and S. Weinfurtner, Nat. Phys. **13**, 833 (2017).
[12] D. Vocke, C. Maitland, A. Prain, F. Biancalana, F. Marino, and D. Faccio, arXiv:1709.04293.
[13] Y. A. Stepanyants and G. H. Yeoh, J. Fluid Mech. **604**, 77 (2008).
[14] A. Andersen, T. Bohr, B. Stenum, J. J. Rasmussen, and B. Lautrup, Phys. Rev. Lett. **91**, 104502 (2003).
[15] V. Cardoso, I. P. Carucci, P. Pani, and T. P. Sotiriou, Phys. Rev. Lett. **111**, 111101 (2013).
[16] A. Coates, M. W. Horbatsch, and T. P. Sotiriou, Phys. Rev. D **95**, 084003 (2017).
[17] S. Hod, Phys. Lett. B **749**, 167 (2015).
[18] S. R. Dolan and D. Dempsey, Classical Quantum Gravity **32**, 184001 (2015).
[19] E. Barausse, V. Cardoso, and P. Pani, Phys. Rev. D **89**, 104059 (2014).
[20] V. Cardoso, J. P. S. Lemos, and S. Yoshida, Phys. Rev. D **70**, 124032 (2004).
[21] E. Berti, V. Cardoso, and J. P. S. Lemos, Phys. Rev. D **70**, 124006 (2004).
[22] S. R. Dolan, L. A. Oliveira, and L. C. B. Crispino, Phys. Rev. D **85**, 044031 (2012).
[23] S. Lepe and J. Saavedra, Phys. Lett. B **617**, 174 (2005).
[24] B. Lautrup, *Physics of Continuous Matter: Exotic and Everyday Phenomena in the Macroscopic World* (CRC Press, Boca Raton, 2004).

[25] L. Rosenhead, Proc. R. Soc. A **127**, 590 (1930).
[26] W. C. Mih, J. Hydraul. Res. **28**, 392 (1990).
[27] G. Vatistas, J. Hydraul. Res. **27**, 417 (1989).
[28] J. E. Hite, Jr. and W. C. Mih, J. Hydraul. Res. **120**, 284 (1994).
[29] O. Bühler, *Waves and Mean Flows* (Cambridge University Press, Cambridge, England, 2014).
[30] R. Schützhold and W. G. Unruh, Phys. Rev. D **66**, 044019 (2002).
[31] V. F. Kopiev and I. V. Belyaev, J. Sound Vib. **329**, 1409 (2010).
[32] C. Coste, F. Lund, and M. Umeki, Phys. Rev. E **60**, 4908 (1999).
[33] V. Cardoso, J. P. S. Lemos, and S. Yoshida, Phys. Rev. D **70**, 124032 (2004).
[34] T. Torres, A. Coutant, S. Dolan, and S. Weinfurtner, arXiv: 1712.04675.
[35] V. Cardoso, A. S. Miranda, E. Berti, H. Witek, and V. T. Zanchin, Phys. Rev. D **79**, 064016 (2009).
[36] See Supplemental Material at http://link.aps.org/supplemental/10.1103/PhysRevLett.121.061101, which includes Refs. [2,33,37–44], for a detailed description of the WKB method, the continued-fraction method, and our numerical simulations, including a comparison among them.
[37] E. W. Leaver, Proc. R. Soc. A **402**, 285 (1985).
[38] H.-P. Nollert, Phys. Rev. D **47**, 5253 (1993).
[39] M. V. Berry and K. Mount, Rep. Prog. Phys. **35**, 315 (1972).
[40] N. Fröman and P. O. Fröman, *Physical Problems Solved by the Phase-Integral Method* (Cambridge University Press, Cambridge, England, 2002).
[41] A. Coutant, R. Parentani, and S. Finazzi, Phys. Rev. D **85**, 024021 (2012).
[42] E. W. Leaver, Phys. Rev. D **41**, 2986 (1990).
[43] W. Gautschi, SIAM Rev. **9**, 24 (1967).
[44] G. B. Cook and M. Zalutskiy, Phys. Rev. D **90**, 124021 (2014).
[45] C. L. Benone, L. C. B. Crispino, C. Herdeiro, and E. Radu, Phys. Rev. D **91**, 104038 (2015).